In vivo imaging of atherosclerotic plaques in apolipoprotein E deficient mice using nonlinear microscopy

Weiming Yu
Indiana University School of Medicine
Department of Medicine
Nephrology Division
Indianapolis, Indiana 46202
E-mail: wmyu@iupui.edu

Julian C. Braz
Lilly Research Laboratories
Indianapolis, Indiana 46285

Ashley M. Dutton
Indiana University School of Medicine
Department of Medicine
Nephrology Division
Indianapolis, Indiana 46202

Pavel Prusakov
Mark Rekhter
Lilly Research Laboratories
Indianapolis, Indiana 46285

Abstract. Structural proteins such as elastin and collagen can be readily imaged by using two-photon excitation and second-harmonic generation microscopic techniques, respectively, without physical or biochemical processing of the tissues. This time- and effort-saving advantage makes these imaging techniques convenient for determining the structural characteristics of blood vessels *in vivo*. Fibrillar collagen is a well-known element involved in the formation of atherosclerotic lesions. It is also an important component of the fibrous cap responsible for structural stability of atherosclerotic plaques. High resolution *in vivo* microscopic imaging and characterization of atherosclerotic lesions in animal models can be particularly useful for drug discovery. However, it is hindered by the limitations of regular microscope objectives to gain access of the tissues of interest and motional artifacts. We report a technique that facilitates *in vivo* microscopic imaging of carotid arteries of rodents using conventional microscope objectives, and at the same time avoids motional artifacts. As a result, collagen, elastin, leukocytes, cell nuclei, and neutral lipids can be visualized in three dimensions in live animals. We present and discuss *in vivo* imaging results using a flow cessation mouse model of accelerated atherosclerosis. [DOI: 10.1117/1.2800337]

Keywords: Second-harmonic generation; intravital microscopy; atherosclerosis; collagen; two-photon excitation; elastin; lipids.

Paper 07095R received Mar. 13, 2007; revised manuscript received May 10, 2007; accepted for publication May 22, 2007; published online Nov. 5, 2007.

1 Introduction

Atherosclerosis is the underlying cause of myocardial infarct, the main cause of death in Western society,[1] and hence it is the primary subject of many ongoing drug discovery efforts.[2] Atherosclerotic lesions consist primarily of macrophages, T cells, and smooth muscle cells, as well as structural components of extracellular matrix including collagen and elastin. Accumulation of neutral lipids (cholesterol esters) in macrophages and extracellular space is a salient feature of atherosclerosis that leads to the formation of the necrotic core retained by a fibrous cap when the lesion becomes mature.[3,4]

Conventionally, drug efficacy is evaluated by postmortem pathology of the arteries in experimental animals, which can be time consuming. Developing *in vivo* imaging modalities would dramatically enhance drug discovery by accelerating analysis, making the evaluation process more objective as well as reducing the number of animals used. Significant efforts and progress have been made in the past few years in applying macroscopic imaging techniques, e.g. magnetic resonance imaging (MRI) and SPECT, to visualize mouse arteries *in vivo*[5–8] as well as microscopic imaging techniques for characterizing arterial walls *ex vivo*.[9,10] However, to better understand the molecular and cellular events associated with the formation of atherosclerotic lesions, microscopic images with submicron and subcellular resolutions *in vivo* are highly desirable.

Therefore, intravital microscopy represents a complementary approach that potentially offers both three-dimensional and high-resolution visualization of a lesion useful for investigations of lesion formation, progress, and understanding the associated molecular and cellular events. However, imaging of atherosclerotic plaques within a major vessel *in vivo* is extremely challenging. The major challenges include the physical restrictions of the microscope objectives, the accessibility of the major blood vessels, and movements associated with the heart beat, breathing, and other animal motions.

To mitigate the problems of sample accessibility, one can use an imaging system with objectives having a stick-like tip and additional degrees of motional freedom (such as the IV100 laser scanning microscope recently developed by Olympus) specifically designed for *in vivo* imaging.[11,12] One practical problem of using such an objective lens is the contact between the optics of the lens with the tissue or blood, which could complicate the measurement processes achieving

Address all correspondence to Weiming Yu, Medicine/Division of Nephrology, Indiana University School of Medicine, 950 W. Walnut St. - R2-268, Indianapolis, IN 46202; Tel: 317 2784481; Fax: 317 2748575; E-mail: wmyu@iupui.edu

1083-3668/2007/12(5)/054008/10/$25.00 © 2007 SPIE

uncompromised performance of the objective lens. Also, it does not eliminate potential artifacts from animal motions, especially imaging at locations near the heart.

On the other hand, *in vivo* imaging using two-photon excitation laser scanning fluorescence microscopes in organ systems such the brain,[13–15] kidneys,[16–18] and small blood vessels of superficial tissue, e.g., the skin,[19] can be achieved without the need of a special objective lens. In previous work, we demonstrated that images of internal organs such as the kidney can be obtained without motional artifacts by stabilizing the tissue, and functional characteristics of the organs and the kinetics of cellular processes can be studied and quantitatively evaluated from these *in vivo* images,[18,20] typically with submicron spatial resolutions. Based on the same idea, in this work we have developed a technique to support and stabilize the artery for obtaining fluorescence and nonlinear microscopic images of atherosclerotic lesions *in vivo*, free of motional artifacts using a two-photon excitation laser scanning microscope.

The use of two-photon excitation microscope systems is beneficial for imaging blood vessels *in vivo* because: 1. elastin, a major structural protein of the blood vessel, produces bright autofluorescent signals under two-photon excitation, and elastin fibers within the vessel wall can be readily imaged[21,22]; 2. collagen fibers produce strong second-order nonlinear effects (second-harmonic generation)[23–27] under high photon flux illumination, a condition similar to that of generating two-photon excited fluorescence, and can be visualized in the microscope with proper barrier filters; 3. the increased penetration depth by the near-infrared excitation light is particularly beneficial for imaging through the vessel wall from outside to reveal the structural features of the atherosclerotic lesions at the luminal side of a vessel, a necessary process for visualizing plaques *in vivo*.

To facilitate *in vivo* imaging of atherosclerotic plaques, we used a carotid ligation model of accelerated atherosclerosis in apolipoprotein E (ApoE)-deficient mice.[28] This model offers fast lesion development in the common carotid artery, a peripherally located vessel with thin walls and simple geometry, which is convenient for *in situ* microscopic imaging. In this work, we explored and demonstrated the feasibility of *in vivo* two-photon excitation fluorescence and second-harmonic imaging of mouse carotid arteries using a conventional microscope objective.

2 Materials and Methods

2.1 *Animal Preparation*

Experimental procedures using animals were approved by the Institutional Animal Care and Use Committees and performed in accordance with the Guide for the Care and Use of Laboratory Animals (Washington, D.C., National Academy Press, 1996). 8-week-old ApoE-KO mice and C57Bl6/J mice were obtained from Taconic (Hudson, New York). The animals ($n=6$ per group) were prefed with a Western diet containing 0.21% cholesterol and 21% fat for 14 days prior to any surgical interventions. To accelerate lesion formation, the left common carotid artery was ligated under isofluorane anesthesia, as described previously.[28] The mice were kept on the same diet postligation surgery. After a desired period of ligation and right before microscopic imaging, animals were anesthetized with an intraperitoneal injection of thiobutabarbital (50 mg/kg) (Sigma, Saint Louis, Missouri), shaved, and placed on a homeothermic table to maintain the body temperature at 37°C. After assuring adequate anesthesia, a 10- to 15-mm longitudinal incision was made at the low neck position along the anterior border of the sternal head of the sternocleidomastoid muscle under sterile conditions. The common carotid artery to be imaged (either left or the right) was exposed by removing the subcutaneous fat tissues and pushing aside the overlying muscles. In experiments when fluorescent dyes were needed, they were infused either via a jugular vein catheter or through the tail vein with a 31 gauge needle insulin syringe. During all procedures, core body temperature of the animal was maintained at 37°C by using a homeothermic table and monitored with a rectal thermometer.

2.2 *Fluorescent Probes*

The fluorescent dye we used for intravenous injection included Nile Red for staining the lipids, and nuclear probe Hoechst 33342, was purchased from Invitrogen (Eugene, Oregon) and used directly by dissolving the dyes in 0.9% saline.

2.3 *Fluorescene Microscopy*

The exposed carotid artery of the animal being imaged was supported by a custom-made stainless steel shovel-like vessel holder, as shown in Fig. 1. On the shovel head there are multiple 500-μm-wide groves about 200 μm in depth for positioning the artery so that a regular 22×50 mm number 1.5 cover glass can be laid flat against the surface of the shovel body. A custom-made stage with a vertical rail having a mechanism for holding the vessel holder horizontally via its handle was placed on top of the sample stage of the Axioplan 2 (upright) microscope base, which is part of the LSM 510 Meta NLO microscope system (Carl Zeiss, Inc., Thornwood, New York) we used. The vertical and horizontal positions of the vessel holder are made adjustable to facilitate positioning of the artery to be imaged. The animal was laid back on a piece of polystyrene foam with a flat surface for comfort.

A 0.5-ml saline solution containing 250 μg of Nile Red with or without 50 μg of Hoechst 33342 was infused through either the tail vein or the jugular vein catheter approximately 10 min before microscopic imaging when imaging the lipids together with or without cellular nuclei, respectively.

In vivo images of the artery from the animals were captured with a two-photon laser scanning fluorescence microscope system (LSM 510 Meta NLO, Carl Zeiss, Inc., Thornwood, New York). The internal and the Meta detectors were configured and used for acquiring fluorescence and second-harmonic signals from 450 to 500 nm (for Hoechst 33342), 500 to 550 nm (for elastin autofluorescence), 560 to 650 nm (for Nile Red), and 388 to 409 nm (for second harmonics) simultaneously, as well as fluorescence emission spectra of the tissues. The polarization of the excitation light is approximately parallel with the orientation of the artery being imaged, and this configuration was used for both the two-photon excitation fluorescence and second-harmonics imaging. A custom-made biochamber was used to cover the whole imaging space around the microscope sample stage, so that the temperature inside the chamber was kept at 37°C. All intravital images were acquired using a $40\times/1.2$ NA water emul-

sions objective. The Ti-sapphire laser (Spectra-Physics, Mountain View, California) was tuned to 800 nm for excitation. The power of the laser was attenuated to between 3 to 30 mW on the sample using an acoustic optical tunable filter (AOTF) of the LSM 510 system. During all imaging procedures, the body temperature of the animal was maintained at 37 °C. After imaging, animals were sacrificed by lethal injection of pentobarbital followed by a bilateral pneumothorax.

2.4 *Histology*

For conventional histology, the mice were perfused and fixed in Zinc-Tris fixative. Paraffin-embedded sections were stained with Masson's Trichrome. Macrophages were immunohistochemically stained using MAC-2 antibody (clone M3/38 from Cedarlane Laboratories, Burlington, North Carolina). Smooth muscle cells were immunostained with anti-α-smooth muscle actin antibody obtained from DAKO (Glostrup, Denmark).

2.5 *Image Data Analysis*

Intravital images were analyzed by using the Meta Imaging Series (version 6, Universal Imaging Corporation, West Chester, Pennsylvania), Zeiss LSM 510 imaging software, and Voxx developed at the Indiana Center for Biological Microscopy.

3 Results and Discussion

Based on conventional histology, no spontaneous lesions occurred in the carotid arteries of the control age-matched mice. In comparison, 14 days after ligation of the left common carotid artery near its bifurcation, atherosclerotic plaque-like lesions were developed along the length of the artery and observed with a cross sectional view under a regular light microscope (Fig. 2). Trichrome staining [Fig. 2(b)] indicates that an extracellular matrix (shown in dark blue) was accumulated predominantly in the peripheral part of the lesion along the lumen side, forming a fibrous cap-like structure. Matrix deposition colocalized with smooth muscle cells [Fig. 2(d)]. The central part of the lesion was occupied by lipid-laden macrophages [Figs. 2(b) and 2(c)]. No lesions were developed in the contralateral common carotid artery Fig. [2(a)], which did not undergo a ligation procedure.

By using the setup described earlier (Fig. 1), we were able to image the carotid artery *in vivo* and effectively eliminate the problem of animal motions. This is demonstrated in various 3-D *in vivo* images of the arteries without signs of motional artifacts. Figure 3 is a 3-D image stack of a normal artery in an orthogonal view showing elastin autofluorescence (in green) and the second-harmonic generation of collagen fibers (in red). No fluorescent dyes were used in the experiment. It can be seen that the elastin fibers are well organized, relatively straight, and aligned approximately parallel with the direction of blood flow. This is consistent with the fact that in major arteries elastin fibers are predominantly longitudinally orientated.[29] The fenestrations of the internal elastic lamina are visible as black holes in the *xy*, *xz*, and *yz* planes, and are most clear in the *xy* plane. The distance between the vessel intima to the outside surface of the vessel in this case is about 60 μm, very close to what is reported in the literature using *ex vivo* imaging.[10] The distribution of the fenestrations appears to extend from the tunica intima through tunica media to the adventitia of the vessel wall. The second-harmonic signals of collagen fibers appear to be primarily located within the adventitia.

To visualize cell nuclei and neutral lipid accumulation *in vivo*, we acquired image stacks of the artery after intravenous infusion of Hoechst dye (nuclear staining) and Nile Red (lipid staining).[30] Elongated smooth muscle cell nuclei within the media as well as the endothelial cells can be clearly observed [Fig. 4(a)]. The smooth muscle cells have an orientation that is perpendicular to the vessel axis, while the endothelial cells are aligned parallel with the longitudinal axis of the carotid artery [Fig. 4(a)], e.g., two cells going through by the blue line in the *xz* plane and three cells slightly below the green line in the *xy* plane are likely to be endothelial cells aligned horizontally (parallel to the vessel). This cellular orientation is as expected for an artery with normal blood flow, since endothelial cells are typically aligned along the direction of the blood flow.[31] On the contrary, in ligated arteries, intimal cells are randomly orientated [Figs. 4(b) and 4(c)], which is consistent with having an altered pattern of blood flow in the vessel. These randomly orientated intimal cells can be the endothelial cells as well as other cell types, including macrophages recruited to the lesion site.

Nonligated arteries, as expected, did not accumulate any neutral lipids [Fig. 4(a)]. However, one week after ligation, we observed small lipid droplets and aggregated clumps of elastin [Figs. 4(b) and 4(c)]. After two weeks of ligation, as the atherosclerotic lesions grew in size [Figs. 5(a) and 5(b)], both the size and number of lipid droplets were increased. Often one can observe lipid cores sandwiched between the two collagen layers (Fig. 5). The atherosclerotic lesion seen in Fig. 5 was developed quite extensively along the vessel as judged by the continuous extensions of the core in the *x* direction [*xz* planes of Figs. 5(a) and 5(b)]. In the *yz* plane, one can see a classical cross section view of the artery containing a plaque (Fig. 5, indicated with white arrows). In comparison, there was more collagen in the vessel ligated for two weeks than that of the controls (Fig. 4).

Remarkably, morphological features of collagen are very different in the fibrous cap as compared to that within the adventitia [Figs. 5(a) and 5(b)]. In the adventitia, collagen can be seen as individual fibers organized in an overall mesh-like structure, as generally observed in the adventitia of arteries.[32] Collagen of the fibrous cap, on the other hand, does not show a clear fiber structure and does not resemble what is observed from that of the adventitia. Since we use second-harmonic generation for collagen visualization, it is reasonable to suggest that the morphological differences we observed here reflect differences in structural organization of the collagen molecules due to the fact that visualization of second harmonics is highly dependent on the structural characteristics of collagen.[26] To the best of our knowledge, this is the first time morphological differences between collagen in the plaque and adventitial collagen are demonstrated *in vivo*. It is still unclear whether the observed structural differences of the plaque collagen reflect the lack of proper fiber maturation or partial degradation of the collagen. Spectroscopic and quantitative analysis are underway to further evaluate the observed morphological or structural differences of collagens.

Fig. 1 Prototype of an artery holder and a setup for *in vivo* imaging of carotid artery.

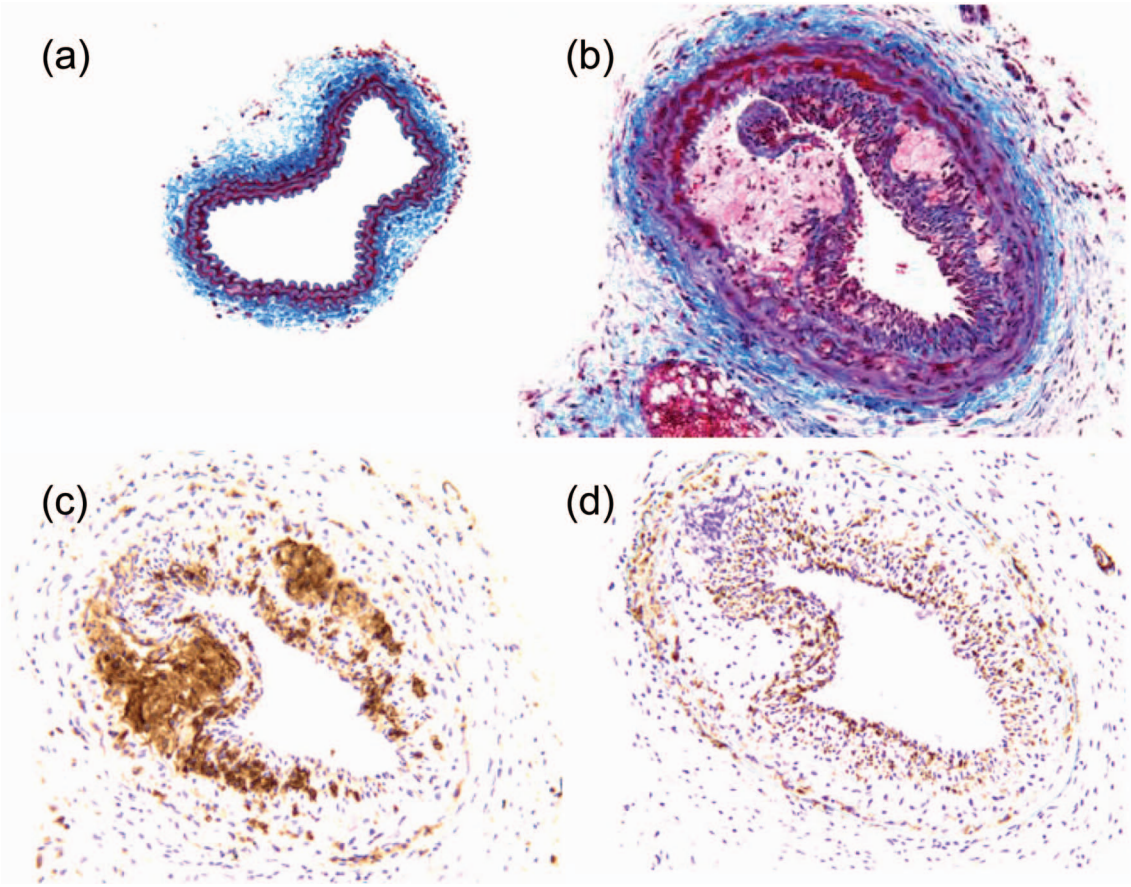

Fig. 2 Lesion development in carotid arteries of ApoE-/- mice. (a) Nonligated artery, Masson trichrome staining; (b) artery 14 days after ligation, Masson trichrome staining showing atherosclerotic lesion with a fibrous cap and lipid core; (c) Mac-2 immunostaining showing macrophages enriched with lipids; and (d) α-actin immunostaining showing actin filaments of smooth muscle cells. Images were acquired with a 20× objective.

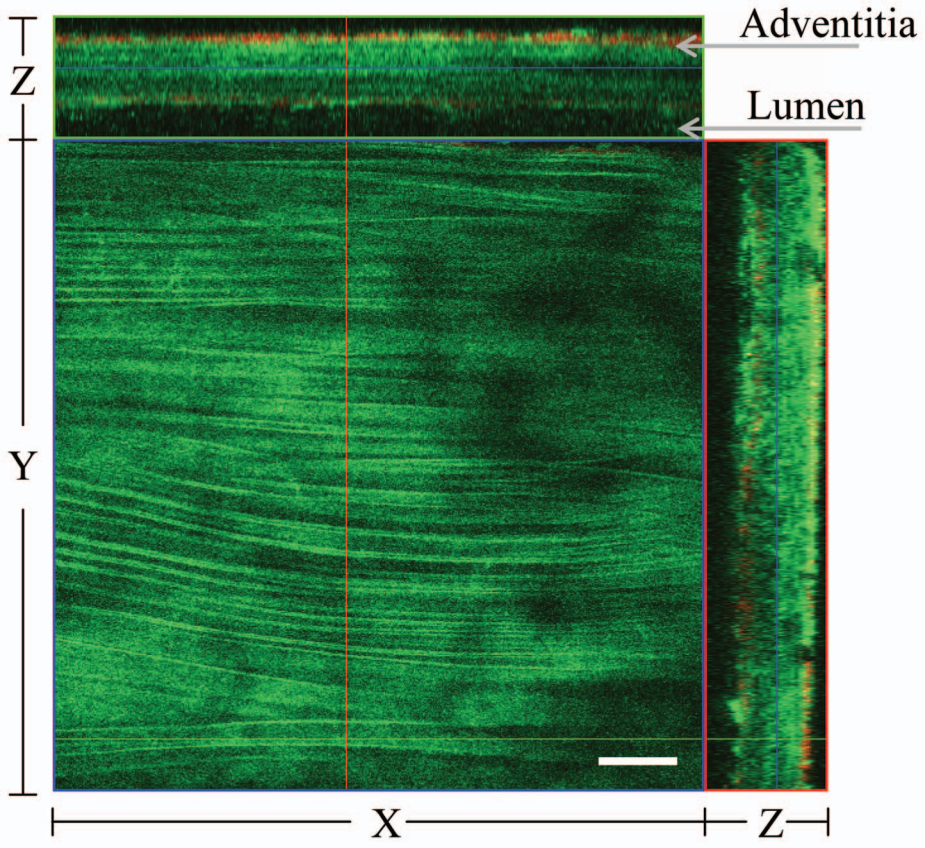

Fig. 3 Orthogonal view of an image stack of a normal carotid artery of ApoE -/- mice. Elastin autofluorescence is shown in green and collagen SHG is shown in red. Image size: $325 \times 325 \times 58\ \mu m^3$. Scale bar: 40 μm.

We have also detected atherosclerotic lesions with large lipid droplets and clumps of elastin, but without the collagen fibrous cap in vessels ligated for two weeks [Fig. 6(a)]. The observations of aggregated elastin are consistent with vessel wall remodeling processes related to lesion formation.[33,34] There are several reasons for the lack of second-harmonic signals in these samples. First, lesion development and maturation could vary in different animals as well as along the length of the same carotid artery.[35] Second, to detect second harmonics, one needs to have a molecule with noncentrosym-

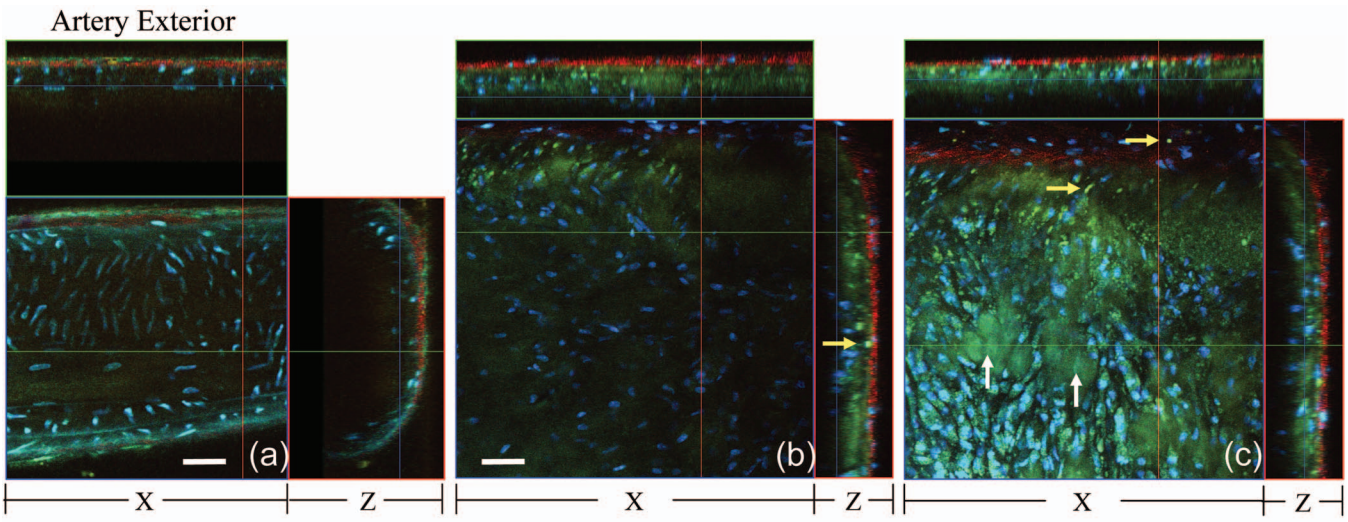

Fig. 4 Cellular orientations of smooth muscle and endothelial cells in normal and ligated carotid artery. (a) Normal artery; (b) intima, artery ligated for one week; and (c) media of the same ligated artery. Cell nuclei in blue, elastin in green, neutral lipids in yellowish green, and collagen (SHG) in red. Yellow arrows indicate lipid droplets. White arrows indicate clumps of elastin. Scale bar: 40 μm.

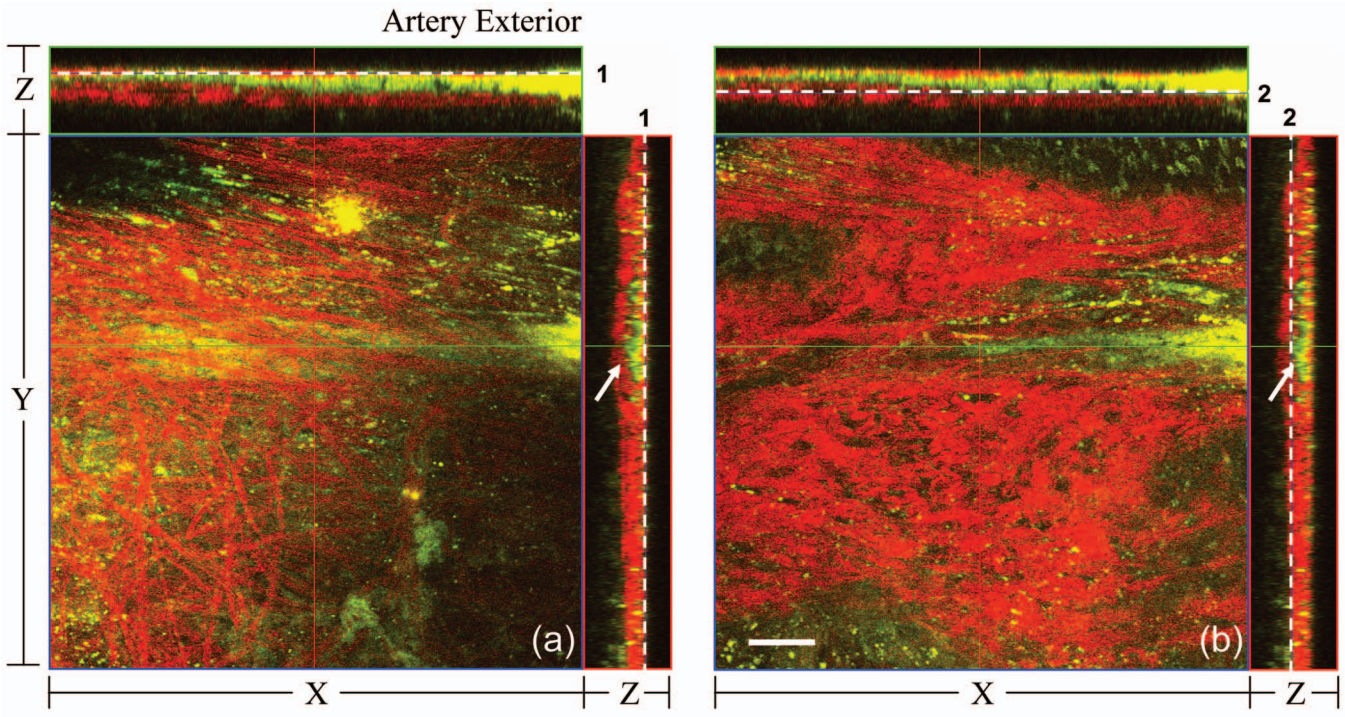

Fig. 5 Orthogonal view of a 3-D image stack showing atherosclerotic lesion of a carotid artery ligated for two week: (a) adventitia, position 1 and (b) intima, position 2. Elastin in green, neutral lipids in yellowish green, and collagen (SHG) in red. *xz* planes showing lipid core extended alone the length of the artery and sandwiched between the two collagen layers. *yz* planes showing a cross section view of the lesion indicated with white arrows. Image size: $325 \times 325 \times 50\ \mu m^3$. Scale bar: 40 μm.

metry that satisfies the phase matching conditions with regard to the molecule interacting with the laser light.[26,36] It is generally agreed that fibrillar (predominantly type 1) collagen is the main source for generating second harmonics,[26,37–39] and mouse atherosclerotic plaques do contain fibrillar collagen.[40] However, newly synthesized collagen may not possess structural features required for generating the second-harmonic signal. Alternatively, the amount of collagen may not be high enough for generating sufficient second-harmonic signals in the backward direction, the detection scheme we can use for *in vivo* applications at the present time.

We have verified spectroscopically that the fluorescence emission spectrum from the lipid droplets (labeled with Nile Red) within the atherosclerotic lesion [Fig. 6(c)] is similar to that from the foam cells found at the lesion site [Fig. 6(b)], and both resemble the spectrum from adipose tissues stained with the Nile Red molecules [Fig. 6(a)].

In a pilot manner, we have also explored if *in vivo* two-photon microscopy is capable of detecting smaller spontaneous lesions in carotid arteries of ApoE-deficient mice. After 12 weeks on the high fat diet (without ligation), we found lipid droplets in both the intima and media [Fig. 7(b) *xz* and *yz* planes]. Other than the smaller size, the images of the spontaneous atherosclerotic lesion resembled those of ligated arteries [Fig. 7(a)]. Interestingly, the adventitial collagen layer [Fig. 7(b) in red] was significantly thicker than that of a normal artery [Figs. 3 and 4(a)]. In fact, the thickening of the collagen layer was observed in both the two-week ligated [Figs. 5 and 7(a)] and nonligated vessels that spontaneously developed atherosclerotic lesions [Fig. 7(b)]. This could be a result of fibrosis known to occur in mice lacking apoE.[41,42] The average thickness of the collagen layer in the arteries that developed atherosclerotic lesions was $14 \pm 2\ \mu$m, measured under our experimental conditions. In comparison, the collagen layer thickness of the normal artery has an average thickness of $8 \pm 2\ \mu$m. We should point out that these measurements are likely to be different from the "native" thickness, since the arteries may have been stretched slightly due to the insertion of the vessel holder.

Macrophages play a critical role in plaque development and destabilization, while neutrophils may be involved in arterial response to injury,[43] hence important in their *in vivo* visualization. Therefore, in separate experiments, we explored *in vivo* imaging of leukocyte accumulation in a mouse carotid artery by using transgenic MacGreen mice expressing enhanced green fluorescence protein (EGFP) in white blood cells.[44] The injury of the vessel wall was induced by acutely overstretching the common carotid artery by gently pulling the artery with a stainless surgical tweezer. Within less than 30 min after stretching the vessel, attachment of green fluorescent leukocyte to the lumen of the vessel was visualized *in vivo* [Figs. 8(a) and 8(b)]. The relative intensity of the elastin fluorescence was considerably lower compared to that of the cells containing GFP [Fig. 8(a) *yz* plane]. In the uninjured vessel, other than occasionally observing a GFP tagged cell flowing through the vessel, there were no cells attached to the vessel wall (data not shown). In these experiments, we were unable to identify white blood cell types, e.g., monocytes and neutrophils. However, this is an important initial

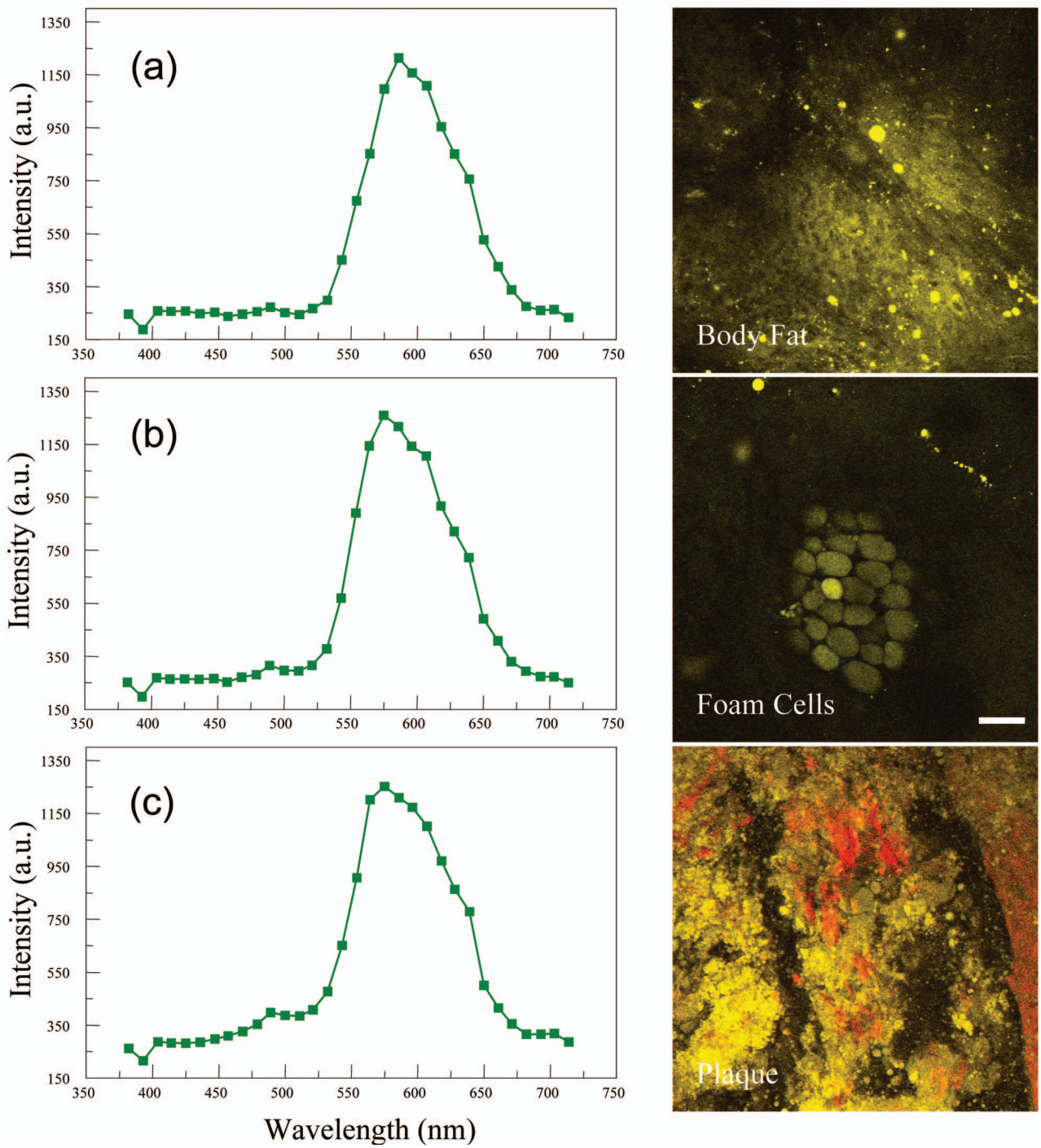

Fig. 6 Fluorescence emission spectra of neutral lipids stained with Nile Red: (a) fat tissue; (b) foam cells; and (c) atherosclerotic plaque, *en face*. Collagen (SHG) in red, neutral lipids in yellow. All samples were freshly isolated and imaged.

step for *in vivo* investigations of vessel wall responses to injury.

Finally, we want to emphasize that *in vivo* imaging facilitated by using a vessel holder provides a unique opportunity to visualize vascular structures in their native states, free from artifacts associated with sample preparation processes. Although one can obtain *ex vivo* images of the vessel wall by using excised arterial specimens [Figs. 9(a) and 9(b)], there are striking differences between the *ex vivo* and *in vivo* images. Specifically, adventitial collagen fibers of excised vessels lost their mesh-like network appearance from intact arteries [as in Fig. 5(a)] and became curled [Fig. 9(a)]. Elastin fibers appeared to be wrinkled and curled in the *ex vivo* images [Fig. 9(a) *xz*,*yz* planes and Fig. 9(b) *xy*, *xz*, and *yz* planes] that were different from those observed *in vivo* (Fig. 3). These differences in the *ex vivo* images are likely to be the results of vessel contraction and elastic recoil associated with

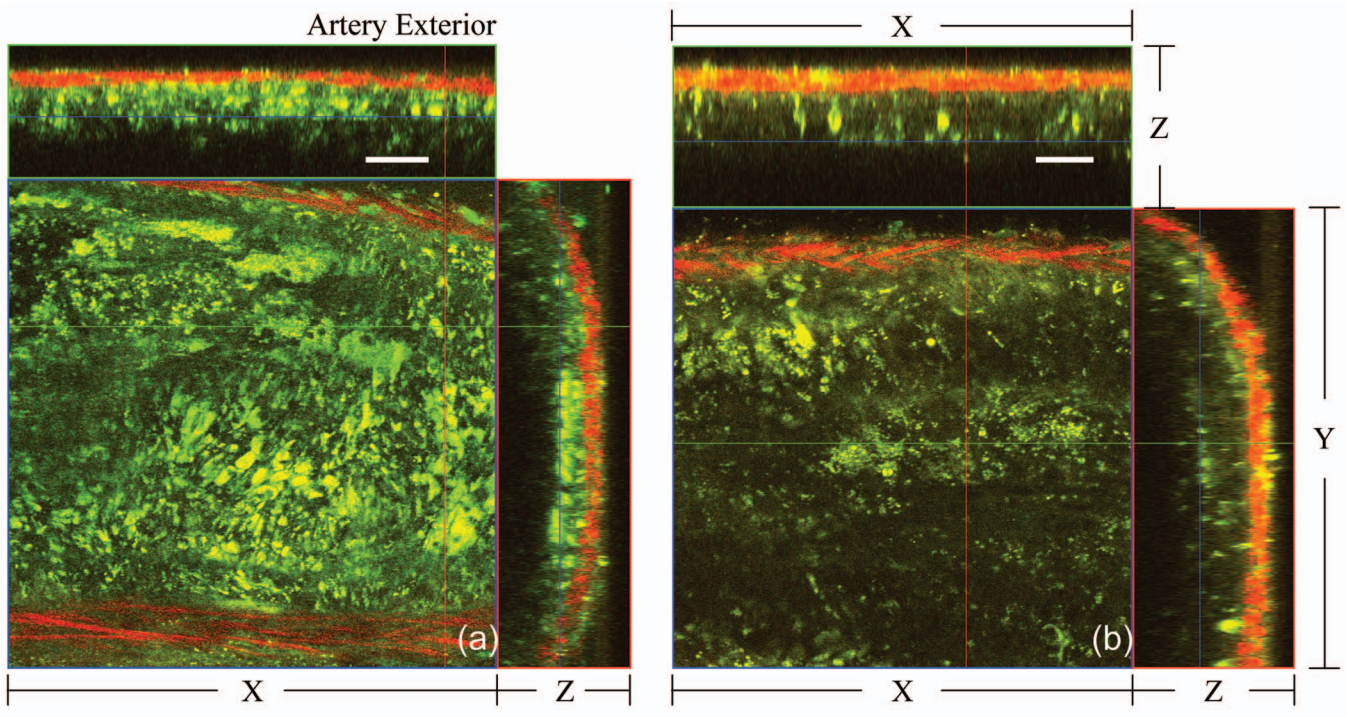

Fig. 7 Comparison between (a) ligated artery and (b) that which developed spontaneous atherosclerotic lesions without ligation. Elastin in green, lipid droplets in yellowish green, and collagen (SHG) in red. Scale bar: 40 μm.

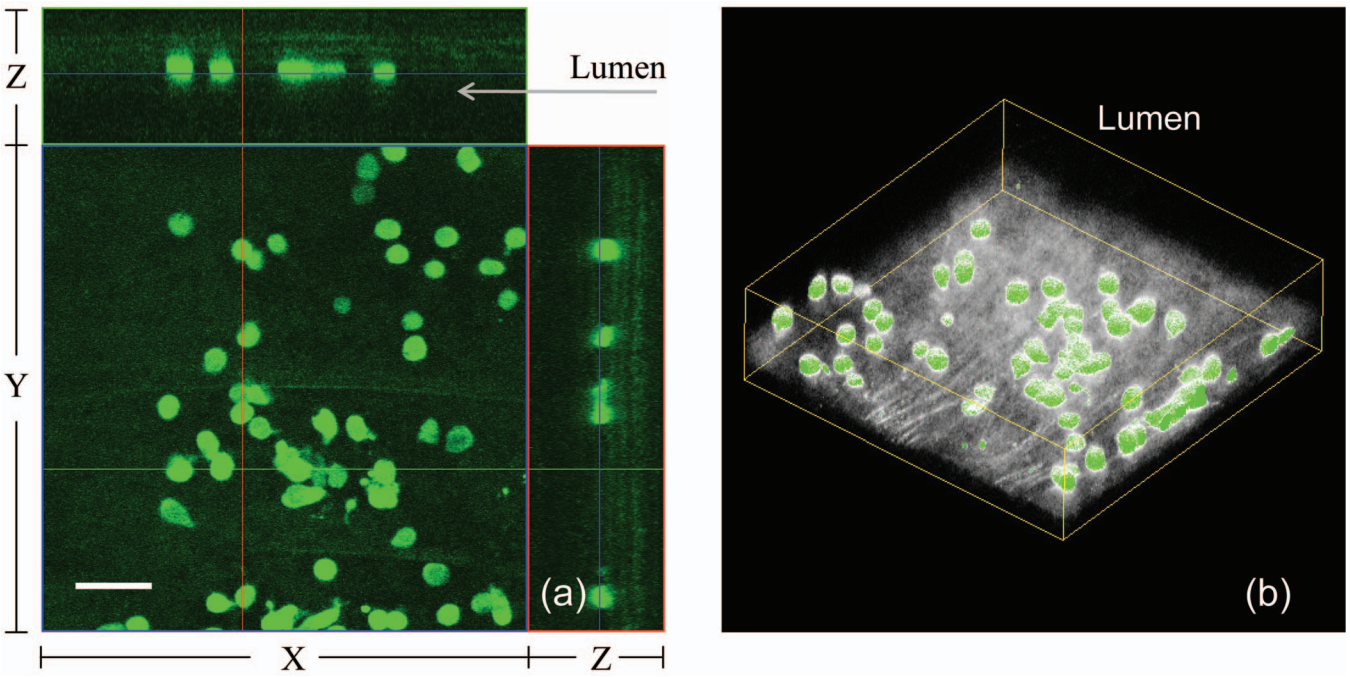

Fig. 8 Luminal accumulations of leucocytes. Images obtained from MacGreen mouse with its leucocytes expressing enhanced green fluorescent protein (EGFP). Leucocytes accumulation was stimulated by acutely overstretching the artery. (a) Orthogonal view of a 3-D image stack. Image size: $230 \times 230 \times 64$ μm^3. Scale bar: 40 μm. (b) 3-D reconstruction of the same dataset showing EGFP-containing leucocytes (in green) and elastin (in white) of the vessel wall extracellular matrix.

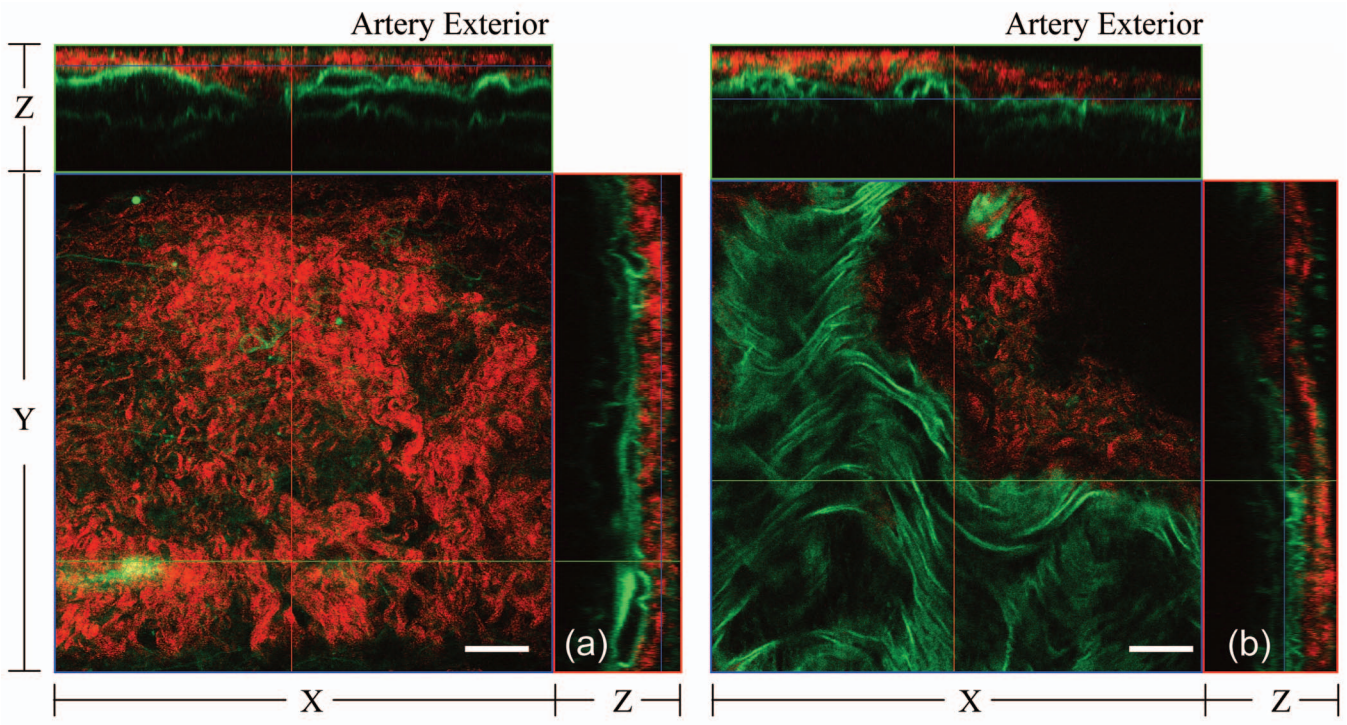

Fig. 9 Orthogonal views of image stacks of *ex vivo* arterial sample of ApoE -/- mice. Elastin autofluorescence is shown in green and collagen SHG is shown in red. (a) *xy* plane closes to the adventitial. (b) *xy* plane closes to the lumen. Scale bar: 40 μm.

excision of the artery. *Ex vivo* microscopy can be a useful alternative, though only when proper sample preparation techniques are used to preserve the native structural features of the arterial wall.

In summary, we have demonstrated that *in vivo* imaging of the carotid arterial wall and obtaining 3-D images without motion artifacts can be achieved using a conventional two-photon confocal microscope with the help of a custom-made vessel holder. We have visualized atherosclerotic lesions in mice with ApoE deficiency using both two-photon excited fluorescence and second-harmonic generation. Critical components of atherosclerotic plaques including collagen, elastin, and neutral lipids can be visualized *in vivo*. This opens up new possibilities for conducting an array of future studies that can answer important questions relevant to vascular diseases. In particular, it will facilitate translational research in drug discovery.

Acknowledgments

The authors wish to thank Simon Atkinson for providing the MacGreen mice as a gift, the Indiana Center for Biological Microscopy for use of its microscopic imaging facility, and Xiao-di Huang for his expert support in histology. The authors also wish to thank Kenneth Dunn and Robert Bacallao for their supports and stimulating discussions. This work was supported by a collaborative research grant from Eli Lilly Research Laboratories (Yu and Rekhter), and a startup fund from an Indiana Genomics Initiative (INGEN) grant from the Eli Lilly and Company Foundation to Indiana University School of Medicine (Yu).

References

1. T. Rodriguez, M. Malvezzi, L. Chatenuod, C. Bosetti, F. Levi, E. Negri, and C. La Vecchia, "Trends in mortality from coronary heart and cerebrovascular diseases in the Americas: 1970-2000," *Heart* **92**(4), 453–460 (2006).
2. C. Q. Meng, "A new era in atherosclerosis drug discovery," *Expert Rev. Cardiovasc. Ther.* **2**(5), 633–636 (2004).
3. H. C. Stary, A. B. Chandler, S. Glagov, J. R. Guyton, W. Insull, Jr., M. E. Rosenfeld, S. A. Schaffer, C. J. Schwartz, W. D. Wagner, and R. W. Wissler, "A definition of initial, fatty streak, and intermediate lesions of atherosclerosis. A report from the Committee on Vascular Lesions of the Council on Arteriosclerosis, American Heart Association," *Arterioscler. Thromb.* **14**(5), 840–856 (1994).
4. H. C. Stary, A. B. Chandler, R. E. Dinsmore, V. Fuster, S. Glagov, W. Insull, Jr., M. E. Rosenfeld, C. J. Schwartz, W. D. Wagner, and R. W. Wissler, "A definition of advanced types of atherosclerotic lesions and a histological classification of atherosclerosis. A report from the Committee on Vascular Lesions of the Council on Arteriosclerosis, American Heart Association," *Circulation* **92**(5), 1355–1374 (1995).
5. S. Vemulapalli, S. D. Metzeler, G. Akabani, N. A. Petry, N. J. Niehaus, X. Liu, N. H. Patil, K. L. Greer, R. J. Jaszczak, R. E. Coleman, C. Dong, P. J. Goldschmidt-Clermont, and B. B. Chin, "Cell therapy in murine atherosclerosis: in vivo imaging with high-resolution helical SPECT," *Radiology* **242**(1), 198–207 (2007).
6. S. Isobe, S. Tsimikas, J. Zhou, S. Fujimoto, M. Sarai, M. J. Branks, A. Fujimoto, L. Hofstra, C. P. Reutelingsperger, T. Murohara, R. Virmani, F. D. Kolodgie, N. Narula, A. Petrov, and J. Narula, "Noninvasive imaging of atherosclerotic lesions in apolipoprotein E-deficient and low-density-lipoprotein receptor-deficient mice with annexin A5," *J. Nucl. Med.* **47**(9), 1497–1505 (2006).
7. E. Trogan, Z. A. Fayad, V. V. Itskovich, J. G. Aguinaldo, V. Mani, J. T. Fallon, I. Chereshnev, and E. A. Fisher, "Serial studies of mouse atherosclerosis by in vivo magnetic resonance imaging detect lesion regression after correction of dyslipidemia," *Arterioscler., Thromb., Vasc. Biol.* **24**(9), 1714–1719 (2004).

8. F. A. Jaffer, M. Nahrendorf, D. Sosnovik, K. A. Kelly, E. Aikawa, and R. Weissleder, "Cellular imaging of inflammation in atherosclerosis using magnetofluorescent nanomaterials," *Mol. Imaging* **5**(2), 85–92 (2006).
9. M. van Zandvoort, W. Engels, K. Douma, L. Beckers, M. Oude Egbrink, M. Daemen, and D. W. Slaaf, "Two-photon microscopy for imaging of the (atherosclerotic) vascular wall: a proof of concept study," *J. Vasc. Res.* **41**(1), 54–63 (2004).
10. R. T. Megens, S. Reitsma, P. H. Schiffers, R. H. Hilgers, J. G. De Mey, D. W. Slaaf, M. G. Oude Egbrink, and M. A. van Zandvoort, "Two-photon microscopy of vital murine elastic and muscular arteries. Combined structural and functional imaging with subcellular resolution," *J. Vasc. Res.* **44**(2), 87–98 (2006).
11. H. Alencar, U. Mahmood, Y. Kawano, T. Hirata, and R. Weissleder, "Novel multiwavelength microscopic scanner for mouse imaging," *Neoplasia* **7**(11), 977–983 (2005).
12. A. N. Pande, R. H. Kohler, E. Aikawa, R. Weissleder, and F. A. Jaffer, "Detection of macrophage activity in atherosclerosis in vivo using multichannel, high-resolution laser scanning fluorescence microscopy," *J. Biomed. Opt.* **11**(2), 021009 (2006).
13. E. J. Yoder and D. Kleinfeld, "Cortical imaging through the intact mouse skull using two-photon excitation laser scanning microscopy," *Microsc. Res. Tech.* **56**(4), 304–305 (2002).
14. M. Oheim, E. Beaurepaire, E. Chaigneau, J. Mertz, and S. Charpak, "Two-photon microscopy in brain tissue: parameters influencing the imaging depth," *J. Neurosci. Methods* **111**(1), 29–37 (2001).
15. R. H. Christie, B. J. Bacskai, W. R. Zipfel, R. M. Williams, S. T. Kajdasz, W. W. Webb, and B. T. Hyman, "Growth arrest of individual senile plaques in a model of Alzheimer's disease observed by in vivo multiphoton microscopy," *J. Neurosci.* **21**(3), 858–864 (2001).
16. K. W. Dunn, R. M. Sandoval, K. J. Kelly, P. C. Dagher, G. A. Tanner, S. J. Atkinson, R. L. Bacallao, and B. A. Molitoris, "Functional studies of the kidney of living animals using multicolor two-photon microscopy," *Am. J. Physiol.: Cell Physiol.* **283**(3), C905–C916 (2002).
17. J. J. Kang, I. Toma, A. Sipos, F. McCulloch, and J. Peti-Peterdi, "Quantitative imaging of basic functions in renal (patho) physiology," *Am. J. Physiol. Renal Physiol.* **291**, F495–F502 (2006).
18. W. Yu, R. M. Sandoval, and B. A. Molitoris, "Quantitative intravital microscopy using a generalized polarity concept for kidney studies," *Am. J. Physiol.: Cell Physiol.* **289**, 1197–1208 (2005).
19. D. R. Larson, W. R. Zipfel, R. M. Williams, S. W. Clark, M. P. Bruchez, F. W. Wise, and W. W. Webb, "Water-soluble quantum dots for multiphoton fluorescence imaging in vivo," *Science* **300**(5624), 1434–1436 (2003).
20. W. Yu, "Quantitative microscopic approaches for studying kidney functions," *Nephron. Physiol.* **103**(2), 63–70 (2006).
21. T. Parasassi, W. M. Yu, D. Durbin, L. Kuriashkina, E. Gratton, N. Maeda, and F. Ursini, "Two-photon microscopy of aorta fibers shows proteolysis induced by LDL hydroperoxides," *Free Radic Biol. Med.* **28**(11), 1589–1597 (2000).
22. A. Zoumi, A. Yeh, and B. J. Tromberg, "Imaging cells and extracellular matrix in vivo by using second- harmonic generation and two-photon excited fluorescence," *Proc. Natl. Acad. Sci. U.S.A.* **99**(17), 11014–11019 (2002).
23. P. J. Campagnola and L. M. Loew, "Second-harmonic imaging microscopy for visualizing biomolecular arrays in cells, tissues and organisms," *Nat. Biotechnol.* **21**(11), 1356–1360 (2003).
24. E. Brown, T. McKee, E. DiTomaso, A. Pluen, B. Seed, Y. Boucher, and R. K. Jain, "Dynamic imaging of collagen and its modulation in tumors in vivo using second-harmonic generation," *Nat. Med.* **9**(6), 796–800 (2003).
25. A. Zoumi, A. Yeh, and B. J. Tromberg, "Imaging cells and extracellular matrix in vivo by using second-harmonic generation and two-photon excited fluorescence," *Proc. Natl. Acad. Sci. U.S.A.* **99**(17), 11014–11019 (2002).
26. R. M. Williams, W. R. Zipfel, and W. W. Webb, "Interpreting second-harmonic generation images of collagen I fibrils," *Biophys. J.* **88**(2), 1377–1386 (2005).
27. S. J. Lin, W. Lo, H. Y. Tan, J. Y. Chan, W. L. Chen, S. H. Wang, Y. Sun, W. C. Lin, J. S. Chen, C. J. Hsu, J. W. Tjiu, H. S. Yu, S. H. Jee, and C. Y. Dong, "Prediction of heat-induced collagen shrinkage by use of second harmonic generation microscopy," *J. Biomed. Opt.* **11**(3), 34020 (2006).
28. E. Ivan, J. J. Khatri, C. Johnson, R. Magid, D. Godin, S. Nandi, S. Lessner, and Z. S. Galis, "Expansive arterial remodeling is associated with increased neointimal macrophage foam cell content: the murine model of macrophage-rich carotid artery lesions," *Circulation* **105**(22), 2686–2691 (2002).
29. J. Nakatake, K. Wasano, and T. Yamamoto, "Three-dimensional architecture of elastic tissue in early atherosclerotic lesions of the rat aorta," *Atherosclerosis* **57**(2–3), 199–208 (1985).
30. P. Greenspan, E. P. Mayer, and S. D. Fowler, "Nile red: a selective fluorescent stain for intracellular lipid droplets," *J. Cell Biol.* **100**(3), 965–973 (1985).
31. B. L. Langille and S. L. Adamson, "Relationship between blood flow direction and endothelial cell orientation at arterial branch sites in rabbits and mice," *Circ. Res.* **48**(4), 481–488 (1981).
32. H. M. Finlay, P. Whittaker, and P. B. Canham, "Collagen organization in the branching region of human brain arteries," *Stroke* **29**(8), 1595–1601 (1998).
33. M. P. Jacob, C. Badier-Commander, V. Fontaine, Y. Benazzoug, L. Feldman, and J. B. Michel, "Extracellular matrix remodeling in the vascular wall," *Pathol. Biol. (Paris)* **49**(4), 326–332 (2001).
34. J. P. Sluijter, D. P. de Kleijn, and G. Pasterkamp, "Vascular remodeling and protease inhibition–bench to bedside," *Cardiovasc. Res.* **69**(3), 595–603 (2006).
35. S. H. Zhang, R. L. Reddick, E. Avdievich, L. K. Surles, R. G. Jones, J. B. Reynolds, S. H. Quarfordt, and N. Maeda, "Paradoxical enhancement of atherosclerosis by probucol treatment in apolipoprotein E-deficient mice," *J. Clin. Invest.* **99**(12), 2858–2866 (1997).
36. L. Moreaux, O. Sandre, and J. Mertz, "Membrane imaging by second-harmonic generation microscopy," *J. Opt. Soc. Am. B* **17**(10), 1685–1694 (2000).
37. B. A. Torkian, A. T. Yeh, R. Engel, C. H. Sun, B. J. Tromberg, and B. J. Wong, "Modeling aberrant wound healing using tissue-engineered skin constructs and multiphoton microscopy," *Arch. Facial Plast. Surg.* **6**(3), 180–187 (2004).
38. A. M. Pena, T. Boulesteix, T. Dartigalongue, and M. C. Schanne-Klein, "Chiroptical effects in the second harmonic signal of collagens I and IV," *J. Am. Chem. Soc.* **127**(29), 10314–10322 (2005).
39. Y. Sun, W. L. Chen, S. J. Lin, S. H. Jee, Y. F. Chen, L. C. Lin, P. T. So, and C. Y. Dong, "Investigating mechanisms of collagen thermal denaturation by high resolution second-harmonic generation imaging," *Biophys. J.* **91**(7), 2620–2625 (2006).
40. E. Lutgens, M. Gijbels, M. Smook, P. Heeringa, P. Gotwals, V. E. Koteliansky, and M. J. Daemen, "Transforming growth factor-beta mediates balance between inflammation and fibrosis during plaque progression," *Arterioscler., Thromb., Vasc. Biol.* **22**(6), 975–982 (2002).
41. K. J. Williams, "Arterial wall chondroitin sulfate proteoglycans: diverse molecules with distinct roles in lipoprotein retention and atherogenesis," *Curr. Opin. Lipidol.* **12**(5), 477–487 (2001).
42. A. Al Haj Zen, G. Caligiuri, J. Sainz, M. Lemitre, C. Demerens, and A. Lafont, "Decorin overexpression reduces atherosclerosis development in apolipoprotein E′-deficient mice," *Atherosclerosis* **187**(1), 31–39 (2006).
43. G. Liuzzo, G. Giubilato, and M. Pinnelli, "T cells and cytokines in atherogenesis," *Lupus* **14**(9), 732–735 (2005).
44. R. T. Sasmono, D. Oceandy, J. W. Pollard, W. Tong, P. Pavli, B. J. Wainwright, M. C. Ostrowski, S. R. Himes, and D. A. Hume, "A macrophage colony-stimulating factor receptor-green fluorescent protein transgene is expressed throughout the mononuclear phagocyte system of the mouse," *Blood* **101**(3), 1155–1163 (2003).